HHS Public Access

Author manuscript

J Soils Sediments. Author manuscript; available in PMC 2023 July 20.

Published in final edited form as:

J Soils Sediments. 2022 June ; 22(6): 1773–1786. doi:10.1007/s11368-022-03171-6.

Soils and spoils: mineralogy and geochemistry of mining and processing wastes from lead and zinc mining at the Gratz Mine, Owen County, Kentucky

James C. Hower[1,2], **Željka Fiket**[3], **Kevin R. Henke**[1,2], **John K. Hiett**[1,2,4], **Jon S. Thorson**[5], **Madan Kharel**[5,6], **Shifeng Dai**[7,8], **Luis F. O. Silva**[9], **Marcos L. S. Oliveira**[9,10]

[1]Center for Applied Energy Research, University of Kentucky, 2540 Research Park Drive, Lexington, KY 40511, USA

[2]Department of Earth and Environmental Sciences, University of Kentucky, Lexington, KY 40506, USA

[3]Division for Marine and Environmental Research, Laboratory of Inorganic Environmental Geochemistry and Chemodynamics of Nanoparticles, Ruđer Bošković Institute, Zagreb, Croatia

[4]Kentucky Ofce of Mine Safety and Licensing, 1025 Capital Center Drive, Frankfort, KY 40601, USA

[5]Department of Pharmaceutical Sciences, University of Kentucky, Lexington, KY 40506, USA

[6]School of Pharmacy, University of Maryland – Eastern Shore, Princess Anne, MD 21853, USA

[7]State Key Laboratory of Coal Resources and Safe Mining, China University of Mining and Technology, Beijing, China

[8]School of Resources and Geosciences, China University of Mining and Technology, Xuzhou 221116, China

[9]Department of Civil and Environmental, Universidad de La Costa, CUC, Universitaria de La Costa, Calle 58 # 55e66, Soledad, Barranquilla, Atlático, Colombia

[10]Faculdade Meridional IMED, Passo Fundo, RS 99070-220, Brazil

Abstract

Purpose—Mineralogical and geochemical features of mining and processing wastes collected in Owen County, part of the Central Kentucky Lead–Zinc district, were investigated. The Gratz mine, abandoned in the 1940s, is on a dairy farm. Aside from discerning the nature of mining refuse at the site, the investigation was part of the University of Kentucky College of Pharmacy's mission to explore unusual environments in the search for unique microbiological communities.

✉James C. Hower, james.hower@uky.edu.

Declarations

Conflict of interest The authors declare no competing interests.

Supplementary Information The online version contains supplementary material available at https://doi.org/10.1007/s11368-022-03171-6.

Materials and methods—Four samples of a soil-plus-spoils mix were collected from spoil piles and two samples, the sluice and coarse samples, were closely associated with the site of the ore processing. Optical petrology (polarized reflected-light, oil-immersion optics at a final magnification of 500 ×), X-ray diffraction, X-ray fluorescence, inductively coupled plasma mass spectrometry, field emission scanning electron microscopy (FE-SEM), and high-resolution transmission electron microscope (HR-TEM) with selected area electron diffraction (SAED) and/or microbeam diffraction (MBD), scanning transmission electron microscopy (STEM), and energy-dispersive X-ray spectrometer (EDS) analyses were employed to characterize the samples.

Results and discussion—Calcite is the main mineral in most samples, followed by near equal amounts of quartz and dolomite. Sphalerite and galena are the principal sulfides and barite is the dominant sulfate. Geochemistry of major elements reflected the mineralogy, whereas trace elements showed different groupings between the minerals. Scandium, Cu, Ga, Ge, Cd, and Sb were found predominantly associated with Zn and Pb and sulfide minerals; Bi, Hf, In, Sn, and Zr with heavy mineral fraction; while the remaining trace elements, including the rare earths, were mostly distributed among other present phases, i.e., oxyhalides, oxides, silicates, and carbonaceous material. The data were used to illustrate the processes and conditions that control the sulfide-mineral oxidation and its potential for the environmental release of associated reaction products.

Conclusions—The wastes represent a potential source of environmentally disruptive concentrations of Zn, Pb, and other sulfide-associated elements. The high share of carbonates suggests near-neutral conditions in deposited wastes, restricting sulfide weathering and further limiting the oxidant activity of Fe. The low-Fe content and its predominant presence in highly resistant hematite also constrain sulfide weathering. Consequently, the spoils have a low potential for generation of acidity and release of heavy metal(loid)s in the surrounding environment.

Keywords

Spoil; Mining waste; Mineralogy; Geochemistry; Pb–Zn mine

1 Introduction

Mining and processing of sulfide ores generate large volumes of waste materials, including the overburden removed during ore mining as well as discard, slurry, and tailings from the preparation, beneficiation, or extraction plants. Spoil is a common term for unwanted or processed material which remains after ore excavation; and although such material is often highly concentrated in metallic compounds or other minerals, their lower amounts make them less viable for extraction. Nevertheless, spoils generated from sulfide ore mining can be active sources of acid generation as well as release points of high concentrations of various metal(loid) s with the potential to severely contaminate soils, surface, and groundwater in the region (Concas et al. 2006; Moncur et al. 2006), even decades after disposal (Moncur et al. 2005; Lindsay et al. 2009; Sheoran et al., 2010). Namely, as global hosts of significant amounts of Cu, Ni, Zn, Pb, and other economically important metals, sulfide ore deposits are also major sources of potentially toxic accessory elements including As, Se, Cd, Sb, and Hg (Moncur et al. 2005, 2009, 2015; Heikkinen et al., 2009; Wuana and Okieimen, 2011; Lindsay et al. 2015). These elements may occur as discrete sulfides or as

trace impurities in other ore and gangue sulfide minerals (Plumlee 1999); and to some extent be enriched in waste materials obtained from mining and processing of sulfide ore.

In addition to enrichment in toxic elements, the spoils can also be characterized by other adverse features such as elevated bioavailability of metals; elevated sand content; lack of moisture; increased compaction; and relatively low organic matter content (Adibee et al. 2013). But the most serious environmental disturbances related to sulfide deposits are caused by the generation of mine drainage (Concas et al. 2006; Moncur et al. 2005, 2006; Lindsay et al. 2009). Spoil wastes run-off, as well as soil erosion, can also contribute to the discharge of significant amounts of dissolved and particulate metals into the environment, representing a persistent and acute pollution source. Contaminated mine drainage (CMD) develops in waste/tailings deposits, where the neutralization capacity of carbonate minerals is low or depleted due to ongoing sulfide-mineral oxidation. On the other hand, neutral mine drainage (NMD) conditions generally persist in tailings where carbonate dissolution effectively neutralizes acid generated by ongoing sulfide-mineral oxidation (Lindsay et al. 2015). In the former conditions, different metals, e.g., Fe, Al, Mn, Zn, Ni, Cu, and Pb, may be released at high dissolved concentrations, while in the latter, weakly hydrolyzing metals including Fe(II); Zn and Cd; and (hydr)oxyanion-forming elements including As, Se, and Sb can be found at elevated levels in surrounding pore waters. The mobility of the released elements further depends upon pH and secondary reactions within tailings/waste deposits (Adibee et al. 2013). Consequently, the extent of environmental impacts associated with waste deposits remaining after sulfide ore mining depends upon their mineralogical and geochemical composition, as well as the in situ chemical, biological, and physical processes (Lindsay et al. 2015).

Within the Central Kentucky Lead–Zinc district, sphalerite and galena were mined from a near-vertical, thin (generally less than 50-cm wide; about 30-cm wide in the Mill shaft, the site of our sampling) calcite and barite veins in the Middle Ordovician Lexington limestone (Miller 1905; Beck 1949; Moore 1977). Owen County, part of the district, was an important producer of ores for over a century, from 1836 at the Union mine to the 1940s at the Gratz mine (Fig. 1) (Norwood 1877; Moore 1977). In addition to the Owen County mines, occurrences of Pb–Zn-mineralized veins were known from the Lockport mine, Henry County (Moore 1977); the Big Twin Creek deposit in Owen County (Beck 1949; Gibbons and Swadley, 1976); the East and West Faircloth mines and the Chinn mine, Woodford and Mercer counties, respectively (Allingham 1972); the Kentron mine, Mercer County (Allingham 1972); and the Hannah Morgan and Twin Chimney mines, Woodford and Mercer counties, respectively (Allingham 1972). The Big Twin Creek, Gratz, and Lockport veins occur along the same trend over distance of about 16 km (Beck 1949). Detailed discussion on the geology of central Kentucky vein deposits can be found in Jolly and Heyl (1964). Miller (1905) described the nearly 100-m vertical Ohio shaft at the Gratz mine as having northward projecting adits at 33- and 66-m depth and a southward-projecting adit at the 33-m level, the latter ending in a tunnel in the cliff above the Kentucky River. The Ohio shaft was in operation at the time of Beck’s (1949) investigation. Lead was mined from the Cedar and Pennyroyal shafts from 1906 to 1913 (Beck (1949). Mining had ceased at the ca. 60-m-deep Mill shaft by the time of Beck’s (1949) report. The processing mill consisted of jaw and roll crushers with the crushed ore being processed in jigs and flotation

cells. Based on Beck's (1949) assessments of the mining operations, it appears as if exact records of the amounts of ore concentrates produced are not available.

This investigation of the mineralogy and geochemistry of the mine and processing refuse was conducted by the University of Kentucky Center for Applied Energy Research (CAER) in collaboration with the University of Kentucky College of Pharmacy's Center for Pharmaceutical Research and Innovation and their mission to explore unusual environments in the search for new and unique microbiological communities. Examples of the results of this collaboration in the study of soils at the sites of coal mine fires and waters from acid mine drainage can be found in Wang et al. (2013, 2014a, b, 2015a, b, 2017a, b) and Shaaban et al. (2013a, b, c, 2017). In this case, the abandoned mine site is located on an active dairy farm.

The specific goal of this study was to evaluate the potential of mining and processing waste material from Owen County for the release of potentially toxic concentrations of metal(loid)s into the environment. The conducted study also seeks to improve our understanding of the mineralogical and geochemical features of mining and processing wastes, which is crucial for estimating the metal sources and possibility of their mobilization, especially in historical mining areas.

2 Materials and methods

2.1 Sampling procedure

Samples of the refuse from mining and processing the Pb–Zn ore were sampled at the site of the Gratz mine, Owen County, Kentucky, on 28 February 2013 (Fig. 1a map). Four samples of a soil + spoils mix were collected from spoil piles (sample numbers 93867 to 93870) and two samples, the sluice and coarse samples, samples 93871 and 93872, respectively, were closely associated with the site of the ore processing. Each sample, as shoveled from the soil or spoil, was collected in in sealable plastic bags in volumes of no less than 5 L. The sampling was from the first ca. 20 cm of soil; the soil extended deeper than the sampling. The archived samples are stored at the Kentucky Geological Survey's Earth Analysis Research Library (EARL), Lexington, Kentucky.

Samples processed and cultured by the University of Kentucky Center for Pharmaceutical Research and Innovation (not included in this contribution) were collected independently at the same sites.

2.2 Petrological, chemical, and mineralogical analysis

Petrology was conducted at the CAER on epoxy-bound particulate pellets prepared to a final 0.05-μm alumina polish. Optical microscopy was conducted on a Leitz Orthoplan microscope with polarized reflected-light, oil-immersion optics at a final magnification of 500 ×. Digital images of the rocks were taken with a Diagnostic Instruments Spot Insight 4 camera.

X-ray diffraction (XRD) analyses at the CAER were performed with a Philips X'Pert diffractometer (model PW3040-PRO) operating at 45 kV and 40 mA. The samples were

ground by hand in a ceramic mortar and pestle, dry mounted in aluminum holders, and scanned at 8–60° 2θ with Cu K-α radiation.

Ash yield was performed according to ASTM D7582–15a (2015) using a Leco 701 thermogravimetric analyzer. Total carbon and sulfur analyses were performed according to ASTM D4239-17 (2017) using a Leco SC-432 carbon/sulfur analyzer. Sulfur forms were analyzed according to ASTM D2491-02(2012) (2012) Ash chemistry at the CAER was analyzed by x-ray fluorescence on a Phillips PW2404 X-ray spectrometer following procedures outlined by Hower and Bland (1989). Samples analyzed at the China University of Mining & Technology – Beijing (CUMT-B) were crushed and ground to pass 200 mesh (75 microns) for geochemical analysis. An elemental analyzer (vario MACRO) was used to determine the percentages of C, H, and N in the soil and refuse samples. X-ray fluorescence (XRF) spectrometry (ARL ADVANT'XP +) was used to determine the content of major elements, expressed as oxides, as outlined by Dai et al. (2012). Inductively coupled plasma mass spectrometry (X series II ICP-MS), in pulse counting mode (three points per peak), was used to determine trace elements in the samples. The ICP-MS analysis and sample microwave digestion programs are outlined by Dai et al. (2011). Samples were digested for ICP-MS analysis using an UltraClave Microwave High Pressure Reactor (Milestone). Multi-element standards (Inorganic Ventures: CCS-1, CCS-4, CCS-5, and CCS-6; NIST 2685b and Chinese standard reference GBW 07,114) were used for calibration of trace element concentrations.

2.3 Nanomineral analysis

Field emission scanning electron microscopy (FE-SEM) and high-resolution transmission electron microscope (HR-TEM) with selected area electron diffraction (SAED) and/or microbeam diffraction (MBD), scanning transmission electron microscopy (STEM), and energy-dispersive X-ray spectrometer (EDS) analyses were conducted following previously reported procedures (Ribeiro et al. 2010; Silva et al. 2011a, b, c; Oliveira et al. 2012; Quispe et al. 2012). To understand nanomineral assemblages, sequential extraction and magnetic separation were conducted following methods from Silva et al. (2012). Because only two-dimensional information is available with those techniques, in this study, we used a dual-beam focused ion beam (FIB), the FEI Dual-Beam™ Helios 600 Nanolab™, equipped with the following primary components: (1) a high-resolution field emission gun (FEG) for SEM; (2) multiple electron detectors for image acquisition, such as through-the-lens detector (TLD), an Everhart–Thornley detector (ETD), and a backscattered electron detector (BSED) for compositional information; and (3) a high-resolution focused Ga^+ ion beam to precisely select, slice, and image a specific region of the species of interest, with a spatial resolution within the 10-nm range. FIB-SEM is an analytical technique based on the unique combination of an ion gun and an electron gun, where specimens can be positioned at the intersection point of the electron and ion beam with an accuracy of much less than 1 nm. This permits simultaneous ion-milling nanosectioning and secondary electron imaging of the region of interest with a spatial resolution within the nanometer range (Giannuzzi and Stevie, 1999).

2.4 Data interpretation and statistical analysis

For purpose of data interpretation, rare earth elements were divided into several groups; the light rare earths (LREE, including elements from La to Gd) and the heavy rare earths (HREE, including elements from Tb to Lu and Y). The normalized REY data (subscript N) refer to upper continental crust values (UCC, Taylor and McLennan 1985), whereas the La_N/Lu_N, La_N/Sm_N, and Gd_N/Lu_N ratios were used for determination of REY enrichment types as defined by Seredin and Dai (2012).

Pearson correlation (r), at significance level $p < 0.05$, was used to examine interactions between variables.

3 Results

What had been the site of the mine shafts and the Pb–Zn ore processing facility (Fig. 1b) is now a wooded hillside on a cattle farm. The shafts are still open, with no fencing or other protection, more than 70 years after the end of the mining (Fig. 1b). The mine refuse, or spoil, piles are vegetated.

3.1 Mineralogy

The bulk mineralogy (Table 1; XRD scans in Supplementary material 1) is generally supported by the chemical analysis (Table 2). Since the country rock is limestone, it is not surprising that calcite is the dominant mineral in most samples. Among the spoil pile samples, samples 93867, 93869, and 93870 were generally composed of calcite > > quartz > > dolomite (or dolomite in similar abundance to quartz) ± illite. Sample 93867 also has sphalerite, zircon, monazite, and galena. The sample 93868 fine spoil more closely resembles the samples from the processing sites, with sphalerite > calcite > barite (Fig. 2a), hokutolite ($(Ba,Pb)SO_4$), galena > quartz, dolomite > hematite (Fig. 2b,c), illite, and yavapaiite ($KFe^{3+}(SO_4)_2$; Fig. 3a). The sluice (processing site) sample 93871 shows a calcite > > quartz > sphalerite, barite, hokutolite > galena, blixite (fluoroblixite)[1] composition and the coarse refuse from the processing site, sample 93872, is composed of calcite > > dolomite, hokutolite > traces of quartz, galena, hematite, and sphalerite.

Sulfide minerals are present as fine minerals dispersed in the country rock (Fig. 4a) but more commonly occur as coarser (several 100 micron) grains (Fig. 4b–d). Considering the known abundance of sphalerite and galena in the samples, the reported forms of sulfur (Table 2) are flawed since the analysis of pyritic sulfur depends on the analysis of Fe (ASTM, 2012). The organic sulfur is, therefore, greatly overestimated and the total sulfur, less the sulfate sulfur, is a reasonable estimate of the sulfur associated with the sulfide minerals. This is particularly important for samples 93898, 93871, and 93872 with S_{total} ranging from 5.93 to 14.30%.

The fine refuse sample 93868, with sphalerite as an important constituent, has 3.57% each of Pb and Zn along with 12.9% Ba (using the CAER XRF results). The sluice (sample 93871)

[1]Blixite is $Pb_8O_5(OH)_2Cl_4$ (http://webmineral.com/data/Blixite.shtml#.Ui4VGD90lv8). Turner and Rumsey (2010) note that other Pb-oxyhalides produce similar X-ray patterns and the firm identification of blixite is difficult. Fluoroblixite has F substitution for the Cl.

and coarse refuse (sample 93872) samples are also enriched in Pb, Zn, Sr, Ba, and Cd. Lead and zinc are present, at least, as sulfides, sulfates, and oxyhalides. Beck (1949) also noted the importance of barite among the vein minerals. Trace substitution in other minerals, such as the carbonate host rock, cannot be discounted, but Pb or Zn carbonates were not found.

Trace elements can occur in the major minerals, such as the Cr-bearing hematite shown in Fig. 2b. Copper-bearing hematite was also noted in TEM investigations of sample 93872 and, as noted above, Pb is a constituent in hokutolite and blixite/fluoroblixite. Lead- and V-enriched carbonaceous material was found in the spoil pile sample 93869 (Fig. 3b). Rare earth elements are not present in significant amounts, despite finds of monazite and zircon in some samples (Fig. 3c).

3.2 Chemical composition of samples

The main chemical properties (loss on ignition (LOI), ash, moisture, and total organic carbon), forms of sulfur, and major oxide and minor element content of the investigated samples are summarized in Table 2. All samples contain high shares of LOI (9.11–35.1%) and ash (95.2–98.9%) and low moisture content (0.12–0.54%). The Si and Ca are the dominant elements, with SiO_2 and CaO in the range 9.5–48.4% and 25.1–48.4%, respectively, which is in accordance with mineralogical analysis and predominance of quartz and calcite in the samples. The highest proportion of these oxides (96.8%) was present in the fine refuse sample 93870 containing very low sulfide content (0.52%). The overall lowest sulfur content was observed in the fine refuse sample 93869, containing the highest LOI (35.1%) and the second highest CaO (42.6%). Contrary to that, the lowest amounts of SiO_2 and CaO were present in the fine refuse (sample 93868), the sluice (sample 93871), and the coarse refuse (sample 93872), i.e., samples with highest sulfur content (5.93–14.3%). These samples also contain the highest concentrations of Zn (up to 5.04%), Pb (up to 3.80%), Sr (up to 3.26%), and Ba (up to 2.79%); using the ICP-MS results.

In general, LOI, sulfur, and moisture, as well as the content of major oxides and minor elements, were found highly variable between the samples, with RSD in the range 21–141% and an average of 63.6%. Thus, based on the investigated parameters, samples taken from spoil piles (samples of fine refuse) cannot be clearly distinguished from the samples taken from the processing site (sluice and coarse refuse samples). Especially worrisome is the fact that some spoil samples, specifically sample 93868, contain the same levels of sulfides as samples from the ore processing site. Namely, sulfide minerals are thermodynamically unstable in the presence of oxygen and water, and their resulting oxidative weathering generates acidity and releases sulfates and associate metal(loid)s to pore waters. Therefore, knowledge of element associations in mineral assemblages in sulfide-enriched mining wastes is critical for anticipating their potential environmental impact. To determine the incidence of certain trace metals in specific mineral phases, the correlation between measured concentrations was studied; whereas the group of rare earth elements was discussed separately in more details.

3.3 Rare earth element distribution

The lanthanide (REE) and REE + Y (REY) data, along with the calculated ratios, anomalies, and fractionation indices, are presented in Table 3. Like other trace elements, the REY concentrations of studied samples were highly variable, with ΣREY ranging from 38.8 to 145 mg kg^{-1} (Table 2). Highest concentrations of REYs were measured in fine refuse (samples 93867) and coarse refuse (sample 93872), up to 3–4 times higher than in other samples, while sluice (sample 93871) exhibited the overall lowest REY concentrations. The Upper Continental Crust normalized REE, shown on Fig. 5 (without Eu, as discussed below), exhibit approximately parallel trends, with relative highs for Sm, Gd, and, in most cases, Tm. Jolly and Heyl (1964) suggested that La, Y, and Yb in the vein calcite were indicators of a deep-seated sources of the mineralizing fluids.

The REY patterns of all the samples showed evidence of LREE enrichment, with LREE/HREE ratios ranging from 3.9 to 4.8, and accounting in average for 80.7%. The La_N/Lu_N, La_N/Sm_N, and Gd_N/Lu_N ratios ranged from 0.8–1.1, 0.79–0.83, and 1.5–2.1, respectively (Table 3). The Y/Ho ratios (29.0–35.4, Table 3) correspond to values reported for sulfides from the Dachang Sn-polymetallic ore field (Guangxi, China) (26.2–33.7, Zhao and Jiang, 2007).

All samples exhibited a lack of cerium anomaly ($Ce_N/Ce_N^* = Ce_N/(0.5La_N + 0.5Pr_N)$ = 0.93–1.04) (Table 3) and a positive to strong positive europium anomaly ($Eu_N/Eu_N^* = Eu_N/(0.67Sm_N + 0.33Tb_N)$ = 2.29–31.5) (formulas after Dai et al. 2016). Yan et al. (2018) showed that overestimation of positive Eu anomalies can be caused by interference from BaO or BaOH during the ICP–MS analysis. According to Yan et al. (2018), only when samples contain Ba/Eu less than 1000, which is the case for samples of fine refuse, samples 93867 and 93870, the interference of Ba on Eu can be ignored. However, if Ba/Eu is > 1000, as in other studied samples, the interfered Eu is highly elevated, resulting in an erroneously high positive Eu_N/Eu_N^* values. This is further supported by the high positive correlation observed between Ba and Eu (c.c. = 1.00), while the same was not the case for other REY elements. Relying only on the Eu anomaly values in samples 93867 and 93870, it can be concluded that the investigated samples are characterized by a positive Eu anomaly, which in combination with $La_N/Sm_N < 1$ and $Gd_N/Lu_N > 1$ points to the M type of enrichment by Seredin and Dai's classification (Seredin and Dai 2012). This type of distribution indicates that REYs are sourced from hydrothermal fluids, which is consistent with low-temperature hydrothermal genesis of Central Kentucky sulfides (Jolly and Heyl 1964) and explains their low abundance in monazite and zircon.

3.4 Element associations

Spearman correlations were used to explore relationships between the studied parameters (Supplementary material 2). Obtained correlation coefficients (r) revealed the grouping of the examined parameters in several groups. The first group consists of S_{tot}, S_{sulf}, S_{org}, Zn, Pb, Sr, Sc, Cu, Ga, Ge, Cd, and Sb which were found highly positively correlated with the r ranging between 0.95 and 1.00. The association of sulfur content and Zn and Pb reflects their common origin in sulfides, while their high correlation with Sr, Sc, Cu, Ga, Ge, Cd, and Sb indicates the predominant presence of these elements in sulfide minerals. The

unusually large quantities of Ge, Cd, and Ga in sphalerites from Central Kentucky mineral district were previously reported by Jolly and Heyl (1964).

The Al_2O_3, K_2O, TiO_2, MnO, and Fe_2O_3 were found to be positively correlated with each other (r from 0.95 to 1.00) and also highly positively correlated with Li, Be, V, Cr, Co, Ni, Rb, Nb, Mo, Cs, REY, Ta, W, Tl, Th, and U (r from 0.95 to 1.00), suggesting their common association in studied samples. The lack of correlation between REY and P additionally demonstrates that REY are not dominantly linked to monazite.

The third group of elements comprises of Bi, Zr, In, and Hf, which were found highly positively correlated with each other (r from 0.90 to 0.99). Tin showed the highest correlation coefficients with Zr ($r = 0.90$), although not statistically significant. Their relationship probably derives from their common origin in heavy minerals, predominantly zircon.

The absence of statistical significance in case of CaO, SiO_2, and Ba probably reflects their dominant presence in carbonates, quartz, and barite, respectively. The positive correlation between MgO and CaO, although not statistically significant, can be explained by their common association in dolomite, further supporting the previous assumption.

4 Discussion

4.1 Environmental impact

The samples with the highest sulfur concentrations (14.3% in 93868, 9.63% in 93871, and 5.93% in 93872, Table 2) exceed both the intervention values of Dutch soil criteria (2000) and the EPA screening levels for industrial soils (EPA 2018) regarding their Zn, Pb, Ba, and Cd content (Table 4). Specifically, levels of Zn and Ba exceed the Dutch intervention values in all samples, while for Pb and Cd, the latter applies for fine refuse samples 93868 and 93869, as well as for the sluice sample 93871 and coarse refuse sample 93872. Copper slightly surpasses the intervention value only in sample 93,868.

While the target values of the Dutch soil criteria (2000) refer to soil quality that fully assists the soil functionalities for the lives of different organisms, the intervention values, on the other hand, indicate the quality for which the functionality of soil is being seriously impaired. Concentrations in excess of the intervention values, which is the case for most of the samples regarding their Zn, Pb, Cd, and Ba content, correspond to contamination and can be considered a serious environmental hazard. The latter is further emphasized by the fact that the Zn, Pb, and Cd are associated with sulfide minerals prone to weathering.

4.2 Sulfide mineral oxidation

The weathering of sulfides in the Owen County poses a risk of acidification and release of significant and environmentally highly disruptive concentrations of major sulfide forming metals (Zn and Pb) as well as elements associated with sulfide minerals, i.e., Ga, Ge, Cu, Cd, and Sb. The obtained mineral and geochemical data were, therefore, used to gain insight into the processes and conditions that control the oxidation of sulfide minerals and the mobility of related reaction products within investigated waste material.

In general, the oxidation of sulfide minerals proceeds with either dissolved oxygen (O_2) or dissolved ferric iron (Fe^{3+}) acting as an oxidizing agent. The oxidation of sphalerite and galena by dissolved oxygen can be described by the reactions 1 and 2. Although none of these reactions generates acid (Seal 2004), the presence of ferric ions can generate significant amount of H^+, as described by reactions 3 and 4. Since the zinc in sphalerite is often partially substituted with Fe (Pring et al. 2008), the oxidation of iron-enriched sphalerite can also contribute to the presence of ferrous iron (reaction 5).

$$ZnS_{(s)} + 2O_2 \rightarrow Zn^{2+} + SO_4^{2-} \quad (1)$$

$$PbS_{(s)} + 2O_2 \rightarrow Pb^{2+} + SO_4^{2-} \quad (2)$$

$$ZnS_{(s)} + 8Fe^{3+} + 4H_2O \rightarrow Zn^{2+} + 8Fe^{2+} + SO_4^{2-} + 8H^+ \quad (3)$$

$$PbS_{(s)} + 8Fe^{3+} + 4H_2O \rightarrow Pb^{2+} + 8Fe^{2+} + SO_4^{2-} + 8H^+ \quad (4)$$

$$(Zn_{(1-x)}Fe_x)S_{(s)} + 2O_2 \rightarrow (1-x)Zn^2 + xFe^2 + SO_4^2 \quad (5)$$

Oxidation of other minerals containing iron, e.g., pyrite or chalcopyrite, can also increase the amount of ferrous ions, while subsequent oxidation of ferrous iron can release additional H^+ (reactions 6 and 7); and dissolved ferric iron can further oxidize the sphalerite, according to reaction 8.

$$Fe^{2+} + \frac{1}{4}O_2 + H^+ \rightarrow Fe^{3+} + \frac{1}{2}H_2O \quad (6)$$

$$Fe^{3+} + 3H_2O \rightarrow Fe(OH)_{3(s)} + 3H^+ \quad (7)$$

$$(Zn_{(1-x)}Fe_x)S_{(s)} + 8Fe_{3+} + 4H_2O \rightarrow (1-x)Zn^{2+} + (8+x)Fe^{2+} + SO_4^{2-} + 8H^+ \quad (8)$$

Compared to dissolved oxygen, the dissolved ferric ion is considered more effective in oxidation of sulfide minerals, but its efficacy ultimately depends on the pH values. While reactions involving ferric ion are favored in acidic conditions, at the near neutral conditions dominates the dissolution by oxygen (Seal 2004).

However, low concentrations of Fe_2O_3 (< 3%) and absence of pyrite or chalcopyrite in investigated samples suggest that the oxidation by ferric iron is rather limited in this case. Additionally, the only iron mineral identified was hematite, present in all samples except in the sluice (sample 93871).

4.3 Carbonate dissolution

Minerals in the host rock generally react to neutralize acid generated via sulfide-mineral oxidation whereby the carbonates are the most reactive ones. In investigated samples, both calcite and dolomite were identified, with calcite as the major carbonate. Mineral dissolution of these minerals consumes H^+, releases divalent cations (Ca and Mg), and generates aqueous carbonate species (Lindsay et al. 2015), as described by the reactions 9 and 10.

$$CaCO_{(s)} + H_{+} \rightarrow Ca^{2+} + HCO_{3} - \quad (9)$$

$$CaMg(CO3)_{2(s)} + 2H^{+} \rightarrow Mg^{2+} + Ca^{2+} + 2HCO_{3} - \quad (10)$$

Following the above, calcite dissolution commonly produces near-neutral porewater pH values (from 6.5 to 7.5; Blowes and Ptacek 1994; Blowes et al. 2003), whereas the pH values approaching 8.0 have been observed in tailings where dolomite and ankerite are the principal carbonates (Blowes et al. 1998; Lindsay et al. 2009). The latter was reported for the sulfide tailings deposits of Greens Creek (Alaska, USA), where the dolomite is the second most abundant component after pyrite and comprises up to 33 wt% of the tailings mineral assemblage. Five years after deposition, the pore water pH in the said tailings deposit ranged from 6.7 to 8.0 (Lindsay et al. 2009). Contrary, in sulfide tailings of the Nickel Rim (Ontario, Canada) and Sherridon (Manitoba, Canada), where the carbonates share is very low (< 0.2 wt% and > 1 wt%, respectively), the acid generated via pyrrhotite oxidation completely depleted carbonate minerals and lowered the pH below 3 within the sulfide-mineral oxidation zone (Johnson et al. 2000; Moncur et al. 2005). Subsequent elevation of the pH in the deeper parts, from 6.5 to 7.0 in the Nickel Rim and up to 5.5 in the Sherridon tailings, was attributed to the dissolution of calcite and ankerite (Johnson et al. 2000; Moncur et al. 2005). Further decrease in the pH values and recorded pH plateaus were to some extent associated with the dissolution of (oxy)hydroxides and silicates, predominant acid-neutralizing reactions following the depletion of carbonates (Lindsay et al. 2015).

4.4 Estimated acidity potential

The acid producing potential (AP) of certain ore waste material is related to its total sulfur content and generally calculated by multiplying the percent of total sulfur by a conversion factor (AP = 31.25 * %S), while its neutralizing effect (NP) is directly proportional to its carbonate content (Seal 2004). The net neutralizing potential (NNP) can be expressed as the ratio of NP to AP (EPA 1994), whereby the ratio < 1 describes the environment more likely to generate acid.

Material from the Owen County, with a sulfide content of 0.5–14.3%, i.e., AP ranging from 15 to 447, and a carbonate content estimated from CaO data (Table 2) ranging from 45 to 86%, has a NNP near or below unity. A high proportion of barite in the samples may cause the over-estimation of AP for the Owen County material, and consequently under-estimation of NNP. However, even with the correction for barite, the NNP remains low.

Despite the low neutralizing potential of the Owen County waste material, there are limiting circumstances for the sulfide dissolution and consequently the release of high, potentially toxic concentrations of elements such as Zn, Pb, Sc, Cu, Ga, Ge, Cd, and Sb. As previously illustrated, the dissolution of the major sulfide phases in the investigated mining and processing wastes is primarily restricted by the presence and share of carbonate minerals. The carbonates not only neutralize the acid generated by sulfide weathering but also limit the influence of Fe on their dissolution by maintaing a near-neutral conditions within the investigated material. Similar observations were reported for the Greens Creek tailings deposits, wherein the shares of carbonates and sulfides are similar, i.e., NNP < 1, but the pore water pH's reflected the near-neutral conditions (Lindsay et al. 2009). Additional constraints for the Owen County material are the relatively low proportion of iron (0.5–3%, Table 2), its predominance in highly resistant hematite, as well as the absence of pyrite or chalcopyrite.

Therefore, the bulk mineralogy in combination with high shares of carbonates most likely condition circumneutral pH conditions within studied wastes, whereby the atmospheric O_2 acts as the principal electron acceptor during sulfide oxidation, similar to the Greens Creek tailings (Lindsay et al. 2009).

However, variability in the composition of similar waste types precludes generalization, and each waste type should be considered separately, taking into account geochemical and mineralogical composition and local hydrogeological and climatological conditions. The large heterogeneity of mineralogical and geochemical features of waste deposits is a function of the rejects being produced and deposited at different times; thus, the reactions between oxygen, water, and minerals such as sulfides, carbonates, and clays happened in different ways, which justifies the variability chemical and mineralogy of waste deposits. The formation of secondary minerals (e.g., Fe and Al-sulfates) and tertiary minerals (e.g., hematite and Al-amorphous phases) that according to previous authors (Silva et al. 2011a, b, c, d, 2021) can be generated according to the intensity of the contact with water (from humidity to rain that further alters the geochemistry of a mining region containing sulfides).

The present study demonstrates that the chemical and mineralogical composition of an abandoned Pb–Zn mining involves complex geochemistry; thus, the present study will help in the environmental recovery of the studied region and in other Pb–Zn mining regions. In future studies, one of the strategies that can be employed is the use of mixtures of industrial, mining, or other wastes to recover the impacts on the environment and human health in mining and Pb–Zn areas. Some authors demonstrate how such a suggestion can be correctly used (Ramos et al. 2017; Ferrari et al. 2019; Cortés et al. 2020).

5 Conclusion

Mining and processing wastes remained decades after the sulfide ore excavation in Owen County, Kentucky, revealed the following characteristics. The mineralogy of samples was found to be dominated by calcite and quartz or dolomite in the same abundance. The geochemical characteristics are reflected in the mineralogy, with major element levels governed by major mineral phases, calcite, dolomite, quartz, and barite. Trace elements, on

the other hand, can be grouped into several groups where sulfides are dominantly enriched in Zn, Pb, Sc, Cu, Ga, Ge, Cd, and Sb. Rare earth elements, despite the presence of monazite and zircon, were related to other mineral phases.

The mineralogical and geochemical features of studied wastes provided a more detailed insight into the ongoing weathering processes. Although the investigated samples contain high shares of sulfides, and consequently high concentrations of elements such as Zn, Pb, Sc, Cu, Ga, Ge, Cd, and Sb, there are limiting circumstances for their release into the enviroment. Namely, the bulk mineralogy of the explored waste material dominated by calcite creates near-neutral conditions in which the dissolution of sulfide phases and consequently the release of high concentrations of potentially toxic elements into the environment are limited.

Supplementary Material

Refer to Web version on PubMed Central for supplementary material.

Acknowledgements

We wish to honor the memory of Alice Marksberry, late of the University of Kentucky Center for Applied Energy Research. Alice had the local connections to get us access to the abandoned sites on what had been her grandfather's farm. She opened doors we could not have easily opened ourselves. We thank our editor and reviewer for their suggestions to improve the manuscript.

References

Adibee N, Osanloo M, Rahmanpour M (2013) Adverse effects of coal mine waste dumps on the environment and their management. Environmental Earth Sciences 70:1581. 10.1007/s12665-013-2243-0

Allingham JW (1972) Geologic map of the Harrodsburg quadrangle, Mercer and Woodford Counties, Kentucky. U.S. Geological Survey Geologic Quadrangle Map GQ-1020, scale 1:24000

ASTM (2012) Standard test method for forms of sulfur in coal. ASTM International, ASTM D2491-02(2012). https://www.astm.org/Standards/D2492.htm

ASTM (2015) Standard test methods for proximate analysis of coal and coke by macro thermogravimetric analysis. ASTM International, ASTM D7582-15a, West Conshohocken, PA, USA. https://www.astm.org

ASTM (2017). Standard test method for sulfur in the analysis sample of coal and coke using high-temperature tube furnace combustion. ASTM International, ASTM D4239-17, West Conshohocken, PA, USA. https://www.astm.org

Beck WA (1949) Investigation of the K.T. Dome zinc-lead mine, Owen and Henry counties, KY. U.S. Bureau of Mines Report of Investigations 4575:10

Blowes DW, Ptacek CJ (1994) Acid-neutralization mechanisms in inactive mine tailings. In: Blowes DW, Jambor JL (eds) The environmental geochemistry of sulfide mine-wastes. Short Course Series 22, Mineralogical Association of Canada, Ottawa, Ontario, Canada, pp 271–291

Blowes DW, Jambor JL, Hanton-Fong CJ, Lortie L, Gould WD (1998) Geochemical, mineralogical and microbiological characterization of a sulphide-bearing carbonate-rich gold-mine tailings impoundment, Joutel, Québec. Appl Geochem 13:687–705

Blowes DW, Ptacek CJ, Jurjovec J (2003) Mill tailings: hydrogeology and geochemistry. In: Jambor JL, Blowes DW, Ritchie AIM (eds) Environmental aspects of mine wastes. Short Course Series Vol. 31, Mineralogical Association of Canada, Ottawa, Ontario, Canada, pp 95–116

Concas A, Ardau C, Cristini A, Zuddas P, Cao G (2006) Mobility of heavy metals from tailings to stream waters in a mining activity contaminated site. Chemosphere 63:244–253 [PubMed: 16216301]

Cortés A, Silva LFO, Ferrari V, Tafferel SR, Feijoo G, Moreira MT (2020) Environmental assessment of viticulture waste valorisation through composting as a biofertilisation strategy for cereal and fruit crops. Environ Pollut 264:114794 [PubMed: 32428819]

Dai S, Graham IT, Ward CR (2016) A review of anomalous rare earth elements and yttrium in coal. Int J Coal Geol 159:82–95

Dai S, Wang X, Seredin VV, Hower JC, Ward CR, O'Keefe JMK, Li T, Li X, Liu H, Xue W, Zhao L (2012) Petrology, mineralogy, and geochemistry of the Ge-rich coal from the Wulantuga Ge ore deposit, Inner Mongolia, China: New data for genetic implications. Int J Coal Geol 90–91:72–90

Dai S, Wang X, Zhou Y, Hower JC, Li D, Chen W, Zhu X, Zou J (2011) Chemical and mineralogical compositions of silicic, mafic, and alkali tonsteins in the late Permian coals from the Songzao coalfield, Southwest China. Chem Geol 282:29–44

Dutch Target and Intervention values (2000) Circular on target values and intervention values for soil remediation. http://www.esdat.net/Environmental%20Standards/Dutch/annexS_I2000Dutch%20Environmental%20Standards.pdf

Ferrari V, Tafferel SR, Espinosa-Fuentes E, Oliveira MLS, Saikia BK, Oliveira LFS (2019) Chemical evaluation of by-products of the grape industry as potential agricultural fertilizers. J Cleaner Production 208:297–306

Giannuzzi LA, Stevie FA (1999) A review of focused ion beam milling techniques for TEM specimen preparation. Micron 30:197–204

Gibbons AB, Swadley WC (1976) Geologic map of the New Liberty quadrangle, Owen and Henry counties, Kentucky. U.S. Geological Survey Geologic Quadrangle Map GQ-1348, scale 1:24000

Heikkinen PM, Räisänen ML, Johnson RH (2009) Geochemical characterisation of seepage and drainage water quality from two sulphide mine tailings impoundments: acid mine drainage versus neutral mine drainage. Mine Water Environ 28:30–49

Hower JC, Bland AE (1989) Geochemistry of the Pond Creek Coal Bed, Eastern Kentucky Coalfield. Int J Coal Geol 11:205–226

Jolly JL, Heyl AV (1964) Mineral paragenesis and zoning in the Central Kentucky mineral district. Econ Geol 59:596–624

Johnson RH, Blowes DW, Robertson WD, Jambor JL (2000) The hydrogeochemistry of the Nickel Rim mine tailings impoundment, Sudbury, Ontario. J Contam Hydrol 41:49–80

Lindsay MBJ, Condon PD, Jambor JL, Lear KG, Blowes DW, Ptacek CJ (2009) Mineralogical, geochemical, and microbial investigation of a sulfide-rich tailings deposit characterized by neutral drainage. Appl Geochem 24:2212–2221

Lindsay MBJ, Moncur MC, Bain JG, Jambor JL, Ptacek CJ, Blowes DW (2015) Geochemical and mineralogical aspects of sulfide mine tailings. Appl Geochem 57:157–177

Miller AM (1905) The lead and zinc bearing rocks of central Kentucky, with notes on the mineral veins. Kentucky Geological Survey Bulletin 2:35

Moncur MC, Ptacek CJ, Blowes DW, Jambor JL (2005) Release, transport and attenuation of metals from an old tailings impoundment. Appl Geochem 20:639–659

Moncur MC, Ptacek CJ, Blowes DW, Jambor JL (2006) Spatial variations in water composition at a northern Canadian lake impacted by mine drainage. Appl Geochem 21:1799–1817

Moncur MC, Jambor JL, Ptacek CJ, Blowes DW (2009) Mine drainage from the weathering of sulfide minerals and magnetite. Appl Geochem 24:2362–2373

Moncur MC, Ptacek CJ, Lindsay MBJ, Blowes DW, Jambor JL (2015) Long-term mineralogical and geochemical evolution of sulphide-rich mine tailings under a shallow water cover. Appl Geochem 57:178–193

Moore FB (1977) Geologic map of the Gratz quadrangle, Owen and Henry counties, Kentucky. U.S. Geological Survey Geologic Quadrangle 1359. 1:24000

Norwood CJ (1877) A reconnaissance report on the lead region of Henry County, with some notes on Owen and Franklin counties. Kentucky Geological Survey, series 2, Reports of Progress 2(7):245–276

Oliveira MLS, Ward CR, French D, Hower JC, Querol X, Silva LFO (2012) Mineralogy and leaching characteristics of beneficiated coal products from Santa Catarina. Brazil Int J Coal Geol 94:314–325

Plumlee GS (1999) The environmental geology of mineral deposits. In: Plumlee GS, Logsdon MJ (eds) The environmental geochemistry of mineral deposits, vol 6A. Society of Economic Geologists. Littleton, CO, USA, pp 71–116

Pring A, Tarantino SC, Tenailleau C, Etschmann B, Carpenter MA, Zhang M, Liu Y, Withers RL (2008) The crystal chemistry of Fe-bearing sphalerites: an infrared spectroscopic study. Am Miner 93:591–597

Quispe D, Pérez-López R, Silva LFO, Nieto JM (2012) Changes in mobility of hazardous elements during coal combustion in Santa Catarina power plant (Brazil). Fuel 94:495–503

Ramos CG, Querol X, Dalmora AC, De Jesus Pires KC, Schneider IAH, Oliveira LFS, Kautzmann RM (2017) Evaluation of the potential of volcanic rock waste from southern Brazil as a natural soil fertilizer. J Cleaner Production 142:2700–2706

Ribeiro J, Flores D, Ward CR, Silva LFO (2010) Identification of nanominerals and nanoparticles in burning coal waste piles from Portugal. Sci Total Environ 408:6032–6041 [PubMed: 20855106]

Seal RR II (2004) Geoenvironmental models for massive sulphide deposits with an emphasis on sedimentary-exhalative lead-zinc deposits. In: Deb M, Goodfellow WD (eds) Sediment-hosted lead-zinc sulphide deposits: attributes and models of some major deposits in India. CRC Press, Australia and Canada, pp 222–245

Seredin VV, Dai S (2012) Coal deposits as potential alternative sources for lanthanides and yttrium. Int J Coal Geol 94:67–93

Shaaban KA, Singh S, Elshahawi SI, Wang XC, Ponomareva LV, Sunkara M, Copley GC, Hower JC, Morris AJ, Kharel MK, Thorson JS (2013b). The native production of the sesquiterpene isopterocarpolone by Streptomyces sp. RM-14–6. Nat Prod Res. 10.1080/14786419.2013.855932

Shaaban KA, Singh S, Elshahawi SI, Wang X, Ponomareva LV, Sunkara M, Copley GC, Hower JC, Morris AJ, Kharel MK, Thorson JS (2013c) Venturicidin C, A new 20-membered macrolide produced by *Streptomyces* sp. TS-2–2. J Antibiot. 10.1038/ja.2013.113

Shaaban KA, Wang X-C, Elshahawi SI, Ponomareva LV, Sunkara M, Copley GC, Hower JC, Morris AJ, Kharel MK, Thorson JS (2013a) Herbimycins D-F, Ansamycin analogues from *Streptomyces* sp. RM-4–15. J Nat Prod 76:1619–1626. 10.1080/14786419.2013.855932 [PubMed: 23947794]

Shaaban K, Saunders MA, Zhang Y, Tran T, Elshahawi SL, Ponomareva LV, Wang X, Zhang J, Copley GC, Sunkara M, Kharel MK, Morris AJ, Hower JC, Tremblay M, Prendergast MA, Thorson JS (2017) Spoxazomicin D and oxachelin C, potent neuroprotective carboxamides from the Appalachian coal fire-associated isolate Streptomyces sp. RM-14–6. J Nat Prod 80:2–11. 10.1021/acs.jnatprod.6b00948 [PubMed: 28029795]

Sheoran V, Sheoran AS, Poonia P (2010) Soil reclamation of abandoned mine land by revegetation: a review. Int J Soil Sediment Water 3/2:13. https://scholarworks.umass.edu/intljssw/vol3/iss2/13

Silva LFO, Izquierdo M, Querol X, Finkelman RB, Oliveira MLS, Wollenschlager M, Towler M, Pérez-López R, Macias F (2011a) Leaching of potential hazardous elements of coal cleaning rejects. Environ Monit Assess 175:109–126 [PubMed: 20490913]

Silva LFO, Oliveira MLS, Neace ER, O'Keefe JMK, Henke KR, Hower JC (2011b) Nanominerals and ultrafine particles in sublimates from the Ruth Mullins coal fire, Perry County, Eastern Kentucky, USA. Int J Coal Geol 85:237–245

Silva LFO, Oliveira MLS, Philippi V, Serra C, Dai S, Xue W, Chen W, O'Keefe JMK, Romanek CS, Hopps SG, Hower JC (2011c) Geochemistry of carbon nanotube assemblages in coal fire soot, Ruth Mullins fire, Perry County, Kentucky. Int J Coal Geol 94:206–213

Silva LFO, Querol X, da Boit KM, deVallejuelo Fdez-Ortiz, Madariaga S, J.M. (2011d) Brazilian coal mining residues and sulphide oxidation by Fenton's reaction: an accelerated weathering procedure to evaluate possible environmental impact. J Hazard Mater 186:516–525 [PubMed: 21145167]

Silva LFO, Sampaio CH, Guedes A, Fdez-Ortiz de Vallejuelo S, Madariaga JM (2012) Multianalytical approaches to the characterisation of minerals associated with coals and the diagnosis of their potential risk by using combined instrumental microspectroscopic techniques and thermodynamic speciation. Fuel 94:52–63

Silva LFO, Santosh M, Schindler M, Gasparotto J, Dotto GL, Oliveira MLS, Hochella MF Jr (2021) Nanoparticles in fossil and mineral fuel sectors and their impact on environment and human health: a review and perspective. Gondwana Res 92:184

Taylor SR, McLennan SH (1985) The continental crust: its composition and evolution. Blackwell, Oxford, p 312

Turner R, Rumsey MS (2010) The minerals of the Mendep Hills and their relationships. Russell Society Journal 13:3–46

US Environmental Protection Agency (1994) Acid mine drainage prediction. Technical Document (EPA 530-R-94-036). U.S. Environmental Protection Agency, Office of Solid Waste. https://www.epa.gov/sites/production/files/2015-09/documents/amd.pdf

US Environmental Protection Agency (2018) Regional screening levels (RSLs). https://www.epa.gov/risk/regional-screening-levels-rsls-generic-tables

Wang X-C, Shaaban KA, Elshahawi SI, Ponomareva LV, Sunkara M, Zhang Y-N, Copley GC, Hower JC, Morris AJ, Kharel MK, Thorson JS (2013) Frenolicins C-F, pyranonaphthoquinones from *Streptomyces* sp. RM-4–15. J Nat Prod 76:1441–1447 [PubMed: 23944931]

Wang X, Elshahawi S, Shaaban K, Fang L, Ponomareva L, Zhang Y, Copley G, Hower J, Zhan C, Kharel M, Thorson J (2014a) Ruthmycin, a novel tetracyclic polyketide from Streptomyces sp. RM-4–15. Org Lett 16:456–459 [PubMed: 24341358]

Wang X, Shaaban KA, Elshahawi SI, Ponomareva LV, Sunkara M, Copley GC, Hower JC, Morris A, Kharel MK, Thorson JS (2014b) Mullinamides A and B, new cyclopeptides produced by the Ruth Mullins coal mine fire isolate Streptomyces sp. RM-27–46. J Antibioti. 10.1038/ja.2014.37

Wang X, Elshahawi S, Shaaban K, Reynolds AR, Ponomareva L, Saunders MA, Elgumati IS, Zhang Y, Copley G, Hower JC, Sunkara M, Morris AJ, Kharel M, Van Lanen SG, Prendergast MA, Thorson J (2015a) Terfestatins B and C, unique *p*-terphenyl glycosides produced by *Streptomyces* sp. RM-5–8. Org Lett. 10.1021/acs.orglett.5b01203.

Wang X, Elshahawi S, Shaaban K, Reynolds AR, Ponomareva L, Saunders MA, Elgumati IS, Zhang Y, Copley G, Hower JC, Sunkara M, Morris A., Kharel M, Van Lanen SG, Prendergast MA, Thorson J (2015b) Correction to Terfestatins B and C, unique p-terphenyl glycosides produced by Streptomyces sp. RM-5–8. Org Let. 10.1021/acs.orglett.5b02788

Wang X, Zhang J, Ponomareva LV, Chen X, Qiu Q, Woodcock R, Elshahawi SL, Chen X, Zhou Z, Hatcher BE, Hower JC, Zhan C-G, Parkin S, Kharel MK, Voss SR, Shaaban KA, Thorson JS (2017a) Mccrearamycins A-D, geldanamycin-derived cyclopentenone macrolactams from an eastern Kentucky abandoned coal mine microbe. Angew Chem 56:2994–2998. 10.1002/anie.201612447 [PubMed: 28140487]

Wang X, Elshahawi SL, Cai W, Zhang Y, Ponomareva LV, Chen X, Copley GC, Hower JC, Zhan G, Parkin S, Rohr J, Van Lanen S, Shaaban KA, Thorson JS (2017b) Bi- and tetracyclic spirotetronates from the coal mine fire isolate Streptomyces sp. LC-6–2. J Nat Prod 80:1141–1149. 10.1021/acs.jnatprod.7b00108 [PubMed: 28358212]

Wuana RA, Okieimen FE (2011) Heavy metals in contaminated soils: a review of sources, chemistry, risks and best available strategies for remediation. ISRN Ecology: Article ID 402647. 10.5402/2011/402647

Yan X, Dai S, Graham IT, He X, Shan K, Liu X (2018) Determination of Eu concentrations in coal, fly ash and sedimentary rocks using a cation exchange resin and inductively coupled plasma mass spectrometry (ICP-MS). Int J Coal Geol 191:152–156

Zhao K, Jiang S-Y (2007) Rare earth element and yttrium analyses of sulfides from the Dachang Sn-polymetallic ore field, Guangxi Province, China: implication for ore genesis. Geochem J 41:121–134

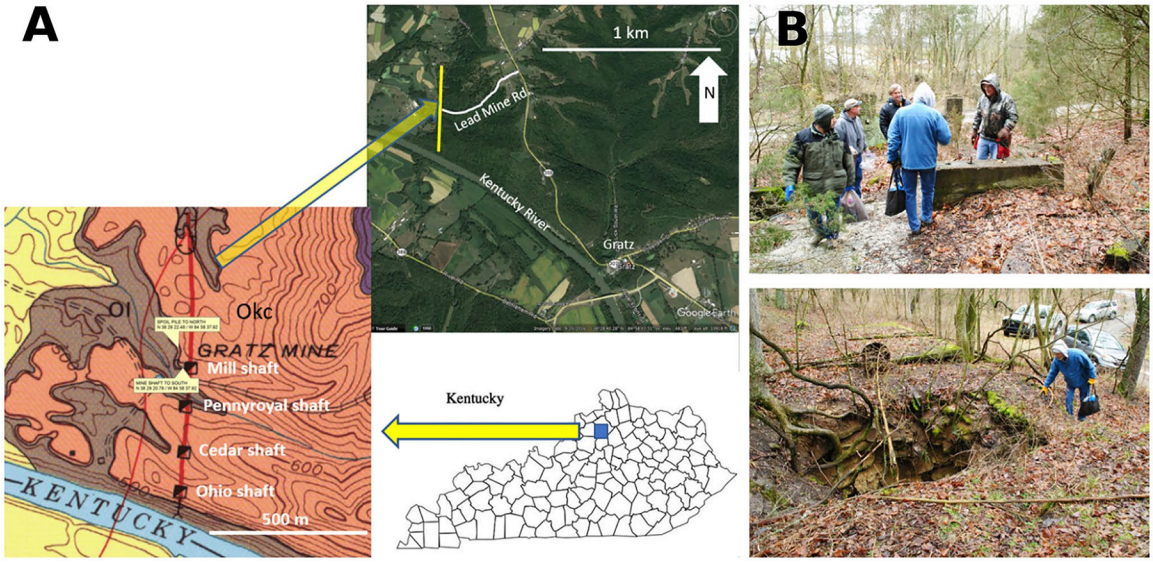

Fig. 1.

A Location of the mine area in Kentucky and of the sample location within the local area. From north to south, the four shafts on the geologic map are the Mill, Pennyroyal, Cedar, and Ohio (after Beck 1949). Inset captions on geologic map (left; from Moore 1977): top — Spoil pile to north: N 38° 29′ 22.48″/W 84° 58′ 37.92″; bottom: Mine shaft (the Mill shaft) to south: 38° 29′ 20.78″/W 84° 58′ 37.92″. The southeast corner of the Google Earth (20 September 2016 image) inset is at N 38° 28′ 57.22′/W 84° 57′ 51.37″ and the northwest corner is at N 38° 30′ 04.62″/W 84° 59′ 09.36″. Formation codes: Ol — Ordovician Lexington Limestone; Okc — Ordovician Kope and Clays Ferry formations (undivided). The contours are labeled in feet (1 foot = 0.3048 m). **B** Top: Ruins of mineral processing facility. Bottom: Abandoned mine shaft

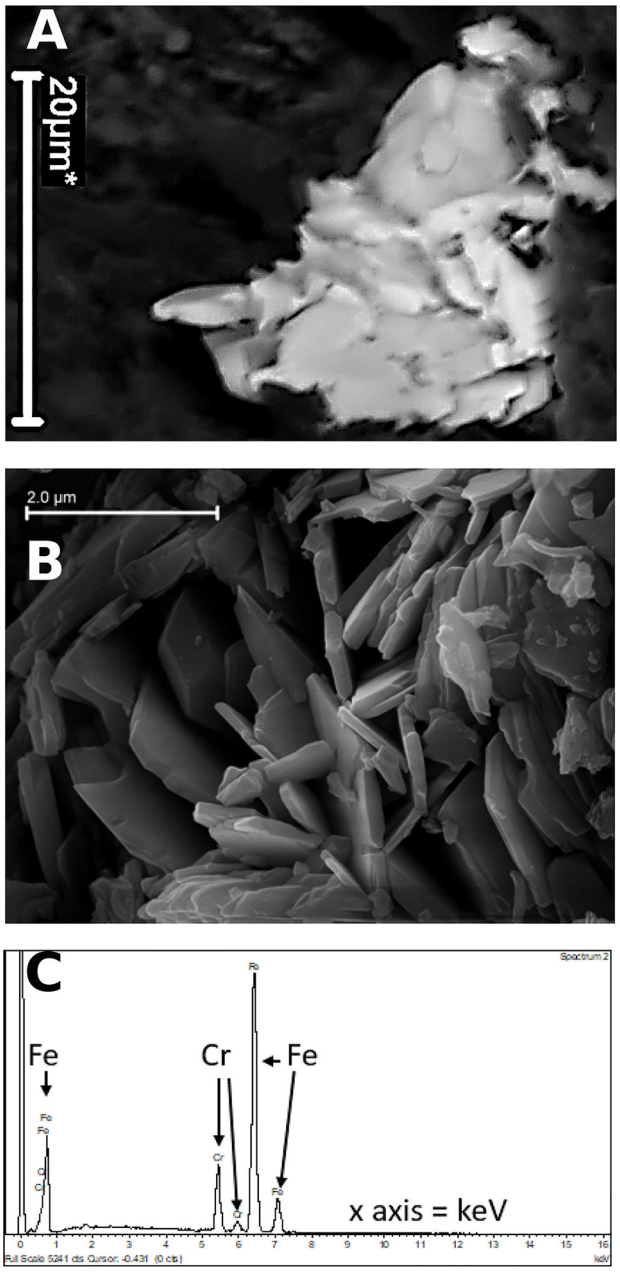

Fig. 2.

A Barite (?) from sample 93871 (SEM image, scale = 20 µm). **B** Cr-bearing hematite from sample 93872 (SEM image, scale = 2 µm). **C** Sample 93872 EDS scan

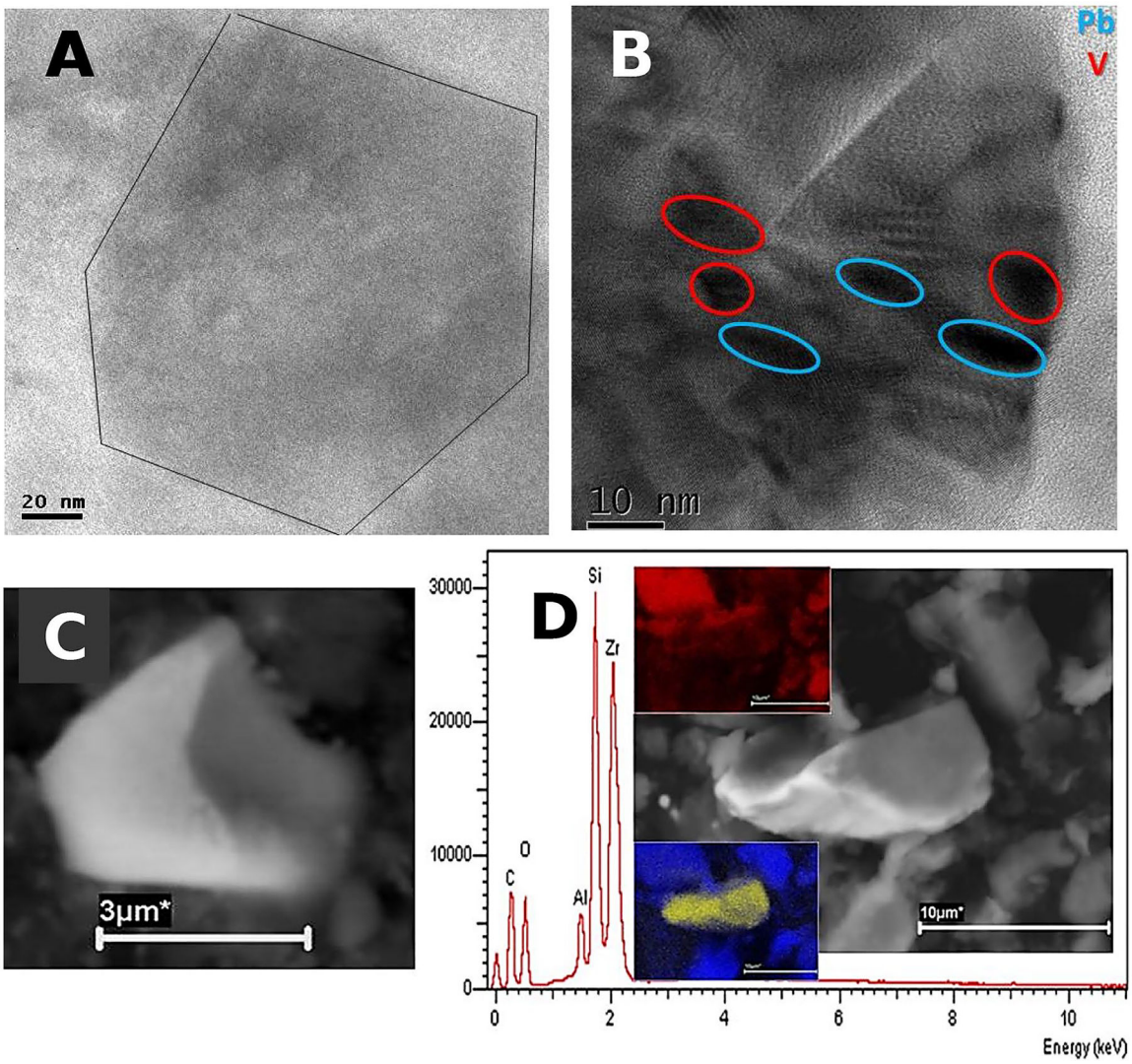

Fig. 3.

A Yavapaiite with characteristic six-sided cross section from sample 93868 (TEM image, scale = 20 nm). **B** Lead- and vanadium-enriched (blue and red ovals, respectively) carbonaceous material from sample 93869 (TEM image, scale = 20 nm). **C** Monazite (sample 93867, scale = 3 µm). **D** Zircon with insets showing Al (top left) and Zr (bottom left) concentrations (sample 93867, scale = 10 µm). All images are from transmission electron microscopy

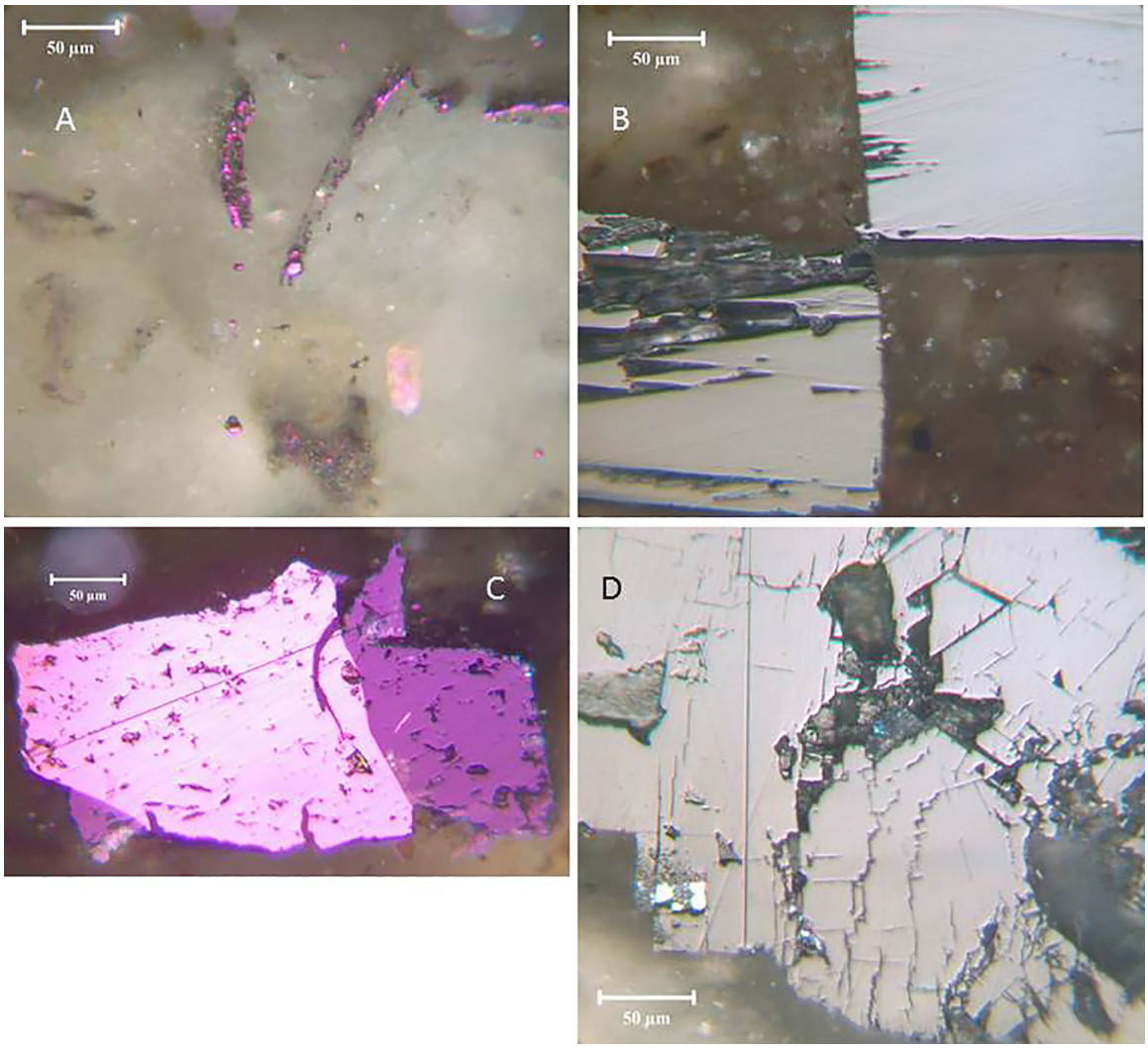

Fig. 4.

Optical microscopy images (oil-immersion, reflected polarized-light, 50 × optics). **A** Sulfides in carbonate matrix. **B** Galena. **C** Sphalerite, **D** Galena. All scales = 50 µm

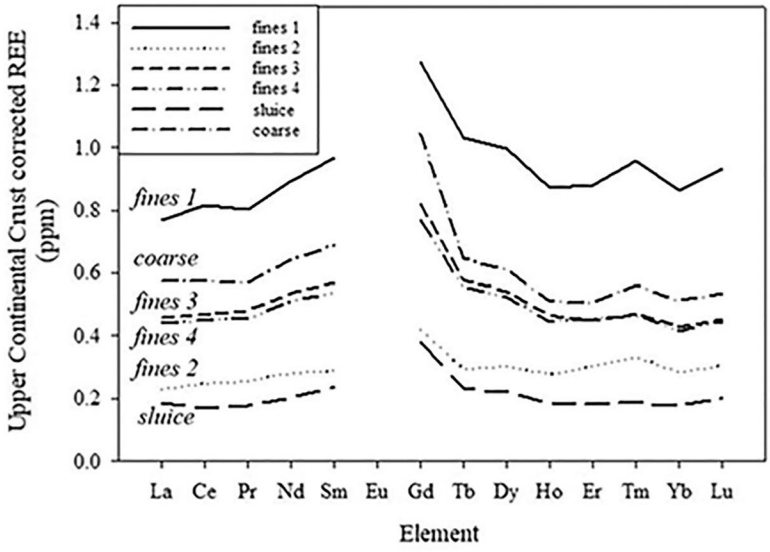

Fig. 5.

Upper continental crust-corrected rare earth element spider plot (corrections after Taylor and McLennan (1985)). The value for Eu is not plotted since the value is not reliable due the interference with Ba, a common constituent in many of these samples

Table 1

Minerals in samples

No	Minerals
93867	Calcite > > quartz > > dolomite, illite, hematite, rutile, sphalerite
93868	Sphalerite > calcite > barite, hokutolite, galena > dolomite, quartz > hematite, illite
93869	Calcite > > dolomite, quartz, hematite
93870	Calcite > > quartz > > dolomite, illite, hematite, sphalerite
93871	Calcite > > quartz > barite, hokutolite, sphalerite > fluoroblixite, galena
93872	Calcite > > dolomite, hokutolite > hematite, galena, mica, sphalerite, barite, quartz, monazite

Table 2

Determined LOI, ash, moisture, fixed carbon, total sulfur, forms of sulfur, major oxides (%) by XRF, and minor elements (mg/kg) by ICP-MS in samples.

No.	LOI	Ash	Moisture	C	S_{tot}	S_{sulf}	S_{org}	S_{py}
93867	27.3	96.0	0.54	11.2	2.68	0.02	2.44	0.22
93868	9.11	98.9	0.12	5.90	14.3	0.54	13.7	0.11
93869	35.1	96.3	0.53	13.0	0.47	0.07	0.21	0.19
93870	32.3	98.3	0.26	12.7	0.52	0.13	0.21	0.18
93871	15.3	95.2	0.54	9.78	9.63	0.32	9.10	0.21
93872	21.9	98.7	0.14	8.67	5.93	0.44	5.31	0.18

No.	SiO_2	TiO_2	Al_2O_3	Fe_2O_3	MgO	CaO	MnO	Na_2O	K_2O	P_2O_5
93867	25.7	0.55	6.59	3.00	1.42	30.2	0.13	0.20	1.98	0.79
93868	2.51	0.07	0.84	0.79	0.69	28.5	0.03	0.00	0.15	0.52
93869	9.50	0.20	3.05	1.26	1.50	42.6	0.06	0.06	0.76	1.03
93870	48.4	0.19	2.63	1.09	1.58	48.4	0.06	0.06	0.63	1.08
93871	4.35	0.10	1.33	1.46	0.73	25.1	0.06		0.30	0.65
93872	13.4	0.26	4.44	2.00	1.24	27.2	0.05		1.14	1.05

No.	Zn	Pb	Sr	Ba	Li	Be	Sc	V	Cr	Co	Ni	Cu
93867	1704	112	1027	5043	15.0	0.90	4.42	31.6	22.1	9.20	17.5	19.9
93868	50398	38008	32616	16578	0.97	0.07	bdl	2.10	2.10	0.75	5.13	197
93869	3903	718	4014	18090	4.77	0.38	1.22	10.9	8.58	2.32	10.8	23.9
93870	1990	469	3068	12879	4.50	0.39	0.92	9.69	7.28	2.44	10.8	20.0
93871	36483	19415	30958	27945	1.99	0.13	bdl	3.79	4.30	1.32	6.67	183
93872	30256	6046	22460	27401	7.24	0.69	2.61	62.8	17.6	5.57	14.6	116

No.	Ga	Ge	Rb	Zr	Nb	Mo	Cd	In	Sn	Sb	Cs
93867	7.67	0.83	47.9	146	7.41	0.49	7.02	0.06	1.22	0.34	2.08
93868	15.9	5.58	3.60	70.0	0.67	0.12	251	0.04	0.75	1.75	0.17
93869	3.94	0.58	18.1	48.9	2.46	0.30	19.7	0.02	0.80	0.33	0.81
93870	3.07	0.49	16.5	44.9	2.30	0.26	10.4	0.01	0.45	0.11	0.73

93871	14.8	3.66	6.04	24.7	0.86	0.29	184	0.03	2.65	0.99	0.28	
93872	13.8	3.25	23.31	78.33	5.28	0.46	165	0.04	1.64	0.75	1.20	

Key: *bdl*, below detection limit

Table 3

Rare earth elements and Y, determined by ICP-MS and expressed in mg/kg, and derived parameters in samples.

	93867	93868	93869	93870	93871	93872
La	23.0	6.85	13.7	13.2	5.57	17.2
Ce	52.2	15.8	29.9	28.7	10.8	36.6
Pr	5.69	1.80	3.41	3.24	1.25	4.04
Nd	23.2	7.28	13.9	13.2	5.28	16.7
Sm	4.35	1.30	2.56	2.42	1.06	3.10
Eu	1.95	3.90	4.61	3.38	6.35	6.51
Gd	4.83	1.59	3.12	2.91	1.45	3.98
Tb	0.62	0.18	0.35	0.33	0.14	0.39
Dy	3.49	1.06	1.89	1.83	0.77	2.14
Y	20.3	6.42	12.6	12.6	5.06	12.6
Ho	0.70	0.22	0.37	0.36	0.15	0.41
Er	2.03	0.69	1.03	1.05	0.42	1.16
Tm	0.29	0.10	0.14	0.14	0.06	0.17
Yb	1.90	0.63	0.94	0.91	0.39	1.12
Lu	0.28	0.09	0.14	0.13	0.06	0.16
ΣREEY	145	47.9	88.6	84.5	38.8	106
LREE/HREE	3.9	4.1	4.1	3.9	4.5	4.8
% LREE	79.6	80.4	80.3	79.4	81.8	82.9
Y/Ho	29.2	29.0	33.9	35.4	34.3	31.1
Eu_N/Eu_N*	2.29	15.7	9.35	7.22	31.5	11.2
Ce_N/Ce_N*	1.04	1.02	1.00	1.00	0.93	1.00
La_N/Lu_N	0.88	0.81	1.08	1.06	0.99	1.15
La_N/Sm_N	0.79	0.79	0.80	0.82	0.79	0.83
Gd_N/Lu_N	1.45	1.48	1.94	1.84	2.04	2.09

EuN* and CeN* calcuated after Dai et al. (2016)

Table 4

Soil concentration ranges and regulatory guidelines for some heavy metals (expressed in mg kg^{-1} or g kg^{-1})

	This study	EPA screening levels[1]	Dutch soil criteria[2]	
		Industrial soil	Target value	Intervention value
Ba	**5043–27,945**	22,000	160	625
Cd	**7.02–251**	98	0.8	12
Co	0.75–9.20	35	9	240
Cr	4.3–22.1	-	100	380
Cu	20.0–197	4700	36	190
Mo	0.12–0.49	580	3	200
Ni	5.1–17.5	1100	35	210
Pb	**112–38,008**	800	85	530
Sb	0.11–1.75	47	3	15
Zn	**1704–50,398**	35,000	140	720

[1] EPA (2018)

[2] Dutch Target and Intervention values (2000)